JOURNAL OF SYNCHROTRON RADIATION
ISSN 1600-5775

Synchrotron X-ray CT characterization of titanium parts fabricated by additive manufacturing. Part II. Defects

Nicola Vivienne Yorke Scarlett,[a]* Peter Tyson,[b] Darren Fraser,[c] Sheridan Mayo[c] and Anton Maksimenko[d]

[a]Mineral Resources, CSIRO, Bayview Avenue, Clayton, Victoria 3168, Australia, [b]Information Management and Technology, CSIRO, Bayview Avenue, Clayton, Victoria 3168, Australia, [c]Manufacturing, CSIRO, Bayview Avenue, Clayton, Victoria 3168, Australia, and [d]Imaging and Medical Beamline, Australian Synchrotron, 800 Blackburn Road, Clayton, Victoria 3168, Australia. *Correspondence e-mail: nicola.scarlett@csiro.au

Received 4 January 2016
Accepted 17 May 2016

Edited by A. Momose, Tohoku University, Japan

Keywords: additive manufacturing; titanium; X-ray tomography.

Synchrotron X-ray tomography (SXRT) has been applied to the study of defects within three-dimensional printed titanium parts. These parts were made using the Arcam EBM® (electron beam melting) process which uses powdered titanium alloy, Ti64 (Ti alloy with approximately 6%Al and 4%V) as the feed and an electron beam for the sintering/welding. The experiment was conducted on the Imaging and Medical Beamline of the Australian Synchrotron. The samples represent a selection of complex shapes with a variety of internal morphologies. Inspection *via* SXRT has revealed a number of defects which may not otherwise have been seen. The location and nature of such defects combined with detailed knowledge of the process conditions can contribute to understanding the interplay between design and manufacturing strategy. This fundamental understanding may subsequently be incorporated into process modelling, prediction of properties and the development of robust methodologies for the production of defect-free parts.

1. Introduction

ASTM has defined additive manufacturing (AM) as 'a process of joining materials to make objects from three-dimensional (3D) model data, usually layer upon layer, as opposed to subtractive manufacturing methodologies; synonyms: additive fabrication, additive processes, additive techniques, additive layer manufacturing, layer manufacturing and freeform fabrication' (Frazier, 2014). The first patent application for such a process was filed in Japan by Hideo Kodama of Nagoya Industrial Research Institute (Kodama, 1981). Unfortunately, Kodama did not file the full patent specification before the one-year deadline after application and consequently the patent was not awarded. Six years later, Charles Hull patented his 'Apparatus for Production of Three-Dimensional Objects by Stereolithography' (Hull, 1986) and is accordingly considered the 'father of 3D printing'. Hull has subsequently been awarded many patents relevant to this technology including the 'STL (stereolithography) file format' which provides suitable model data *via* triangulated surfaces and slicing.

AM technologies are applicable to a wide range of materials (polymers, ceramics and metals) and provide unprecedented design freedom and rapid prototyping opportunities. In 2009 a group of 65 recognized leaders in the field of freeform processing met for the 'Roadmap for Additive Manufacturing (RAM) Workshop: Identifying the Future of Freeform Processing' (Bourell *et al.*, 2009). The goal of this was to

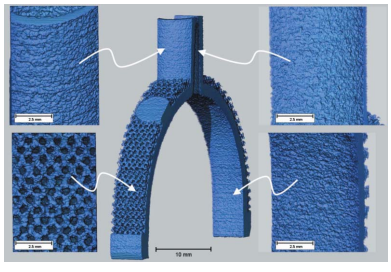

'develop and articulate a roadmap for research in the area of additive manufacturing for the next 10–12 years'. The main recommendations of the workshop focused on design; process modelling and control; materials, processes and machines; biomedical applications; and energy and sustainability applications. Underpinning many of these goals was the need for fundamental understanding to enable the development of predictive models based on process–structure–property relationships. The development of such predictive models will rest upon the relation of detailed materials characterization with design and processing parameters gained where possible *in situ* (Gatto & Harris, 2011) but of necessity more frequently 'post mortem'.

This paper describes the results of synchrotron X-ray tomography (SXRT) inspection of a number of titanium parts produced with Arcam's EBM® (electron beam melting) system. The pieces examined cover a range of functions and design specifications. The use of X-ray tomography, either laboratory or synchrotron, is not routine but its applicability and potential for process feedback have been demonstrated (Léonard *et al.*, 2012; Tammas-Williams *et al.*, 2015; Van Bael *et al.*, 2011). A non-destructive technique like SXRT provides a number of qualitative and quantitative measurements from a single non-destructive experiment.

2. Experimental

The pieces examined here were made from powdered titanium alloy, Ti64 (Ti alloy with approximately 6%Al and 4%V) with an approximate particle size of 45–106 µm with a median d_{50} particle size of 70 µm. The Arcam process[1] is a metal 3D printing process conducted at elevated build temperatures in a vacuum. It uses an electron beam to heat a powder layer raked over a start plate to a temperature that lightly sinters the layer and then melts and fuses the powders in the shape required for that layer. The plate is then lowered 50 µm into a tank and a new layer of powder is deposited on top by the rake. Heating and melting is repeated and a new fused layer is formed on top of the previous one with the overlapping parts melted together. This is repeated many times until 3D parts are created. The sample suite comprised functional and test pieces including a tag for the tracking of big fish, the acetabular cup component of an artificial hip joint, a solid rectangular piece, and thick- and thin-walled sections of flexible hosing. The pieces had very different functionalities and therefore presented a range of design challenges.

The fish tags needed to be able to pierce the fish's skin easily and then to be retained for as long as possible. AM was ideal for such a project where a range of designs could be rapidly produced and trialled. Titanium was an ideal material for such an application as it is strong, resistant to the corrosiveness of the marine environment and is biocompatible.

[1] The specifics of the process used in the manufacture of these samples are Arcam software process themes 3.2.121; 50 µm layers; melt theme (hatching) speed function 98; two contours inner and outer and offset to contour 0.05 mm.

The acetabular cup was a sizeable solid piece with a rough exterior to assist with bone growth onto or into the porous surface. The biocompatibility of titanium was also a key element in its choice for this piece. The flexible hose sections presented design challenges in the thickness of the walls, the proximity of the surfaces and the need for unsupported manufacture of their complex shapes. The solid rectangular piece was built with the aim of investigating conditions for the production of large flat areas.

2.1. Synchrotron data collections

Experiments were conducted in Hutch 3B of the Imaging and Medical Beamline (IMBL) (Stevenson *et al.*, 2012) at the Australian Synchrotron using the 'Ruby' detector.[2] This detector is a single pco.edge sensor, lens-coupled scintillator with minimum and maximum fields of view of 15.3 mm × 12.9 mm and 141 mm × 119 mm, respectively. The pixilation is 2560 × 2160 and the image pixel size is between 6 and 55 µm depending on the field of view. Data may be collected at up to 50 frames s^{-1}. A detector-to-sample position of ∼1 m was used. The field of view in this experiment was ∼30 mm × 15 mm. Data were collected at the highest available pixel size of 11.3 µm using monochromatic X-rays of energies between 50 and 100 keV. Note that this gives a spatial resolution of approximately 2–3 times this, *i.e.* ∼20–30 µm.

The pieces were positioned vertically on the sample stage such that their centre of rotation kept the region of interest within the field of view of the detector. The tomographic scan was collected over a 180° range in 0.1° steps, making 1800 views in total, with an exposure time of 0.6 s per view.

2.2. Data analysis

For each sample 1800 radiographs were reconstructed into orthogonal slices using the *X-TRACT* software (Thompson *et al.*, 2012) on the MASSIVE supercomputer cluster (Goscinski *et al.*, 2014). A tomographic slice from one of the fish tag datasets is shown in Fig. 1. The reconstructed slices were then imported as volumes and rendered for visualization and measurement using *AvizoFire*® software (Visual Sciences Group).

3. Results and discussion

Tomographic imaging of the samples shows the clear variation in the surface morphology depending upon the design of the piece and the direction of manufacture. The final (upper) surfaces of the pieces are smooth in comparison with the sides and lower surfaces which have well preserved spherical morphologies of the original powder (Fig. 2). Surface roughness reduces ultimate tensile strength (UTS) and yield strength *via* fracture initiation from surface imperfections. Chemical etching to reduce surface roughness improves these properties to values comparable with machined specimens. This, however, may not be achievable for intricate parts which

[2] Additional details of this detector are given in Part I of this work (Scarlett *et al.*, 2016).

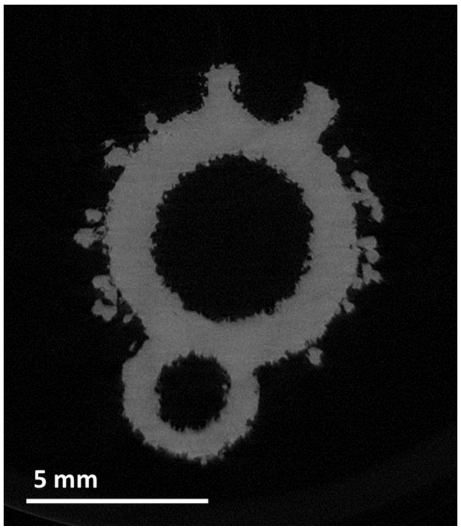

Figure 1
Reconstructed slice from the fish tag dataset.

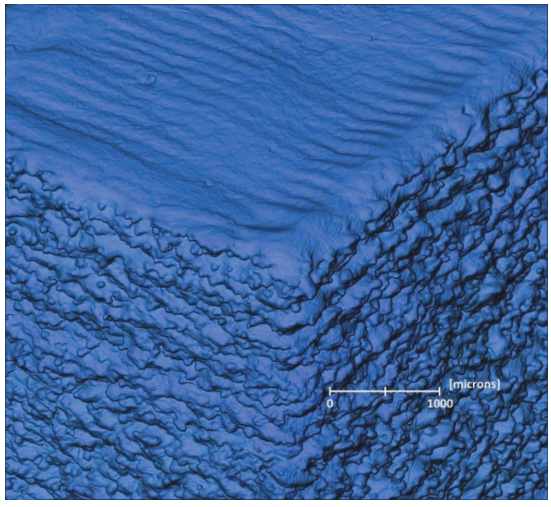

Figure 2
Tomographic image of a solid piece of an AM titanium block showing the smooth finish of the final surface in contrast to the retained powder morphology of the layers as viewed from the side.

contain complex interior structures (Sun *et al.*, 2016). Reconstructed slices through the volumes generally show solid material with very little (less than 1%) porosity (Fig. 1).

3.1. Fish tag

The fish tag was manufactured from the base to the point as shown in Fig. 3. The surface finish on the top conical portion has regular evenly spaced deposition layers with some retained powder morphology. The coarse pattern on the outside of the main body of the tag is a designed protuberance, the upper surface of which is effectively a 'final' surface and has the characteristic smooth features of such (Fig. 4). The retained powder morphology of the main body surface is much less on these features.

The cylindrical section extensions on the sides of the tag base slope upwards from the outer to the inner edge (Fig. 5). These surfaces show clearly the change in finish from the

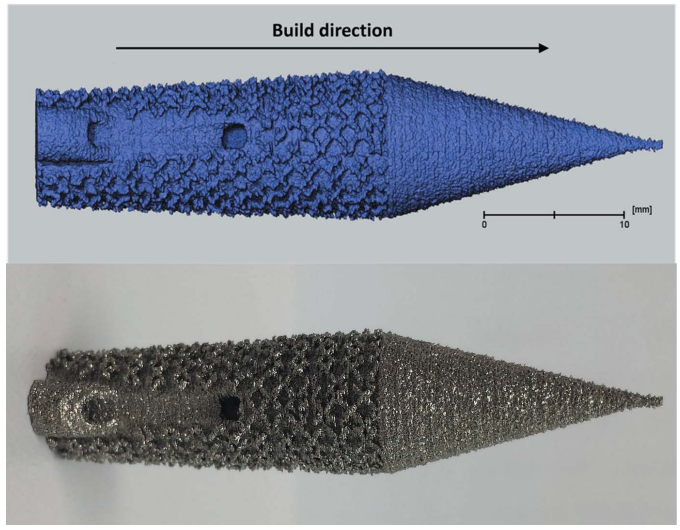

Figure 3
Stitched image of five Z levels collected for the fish tag (top) with an equivalent optical image below.

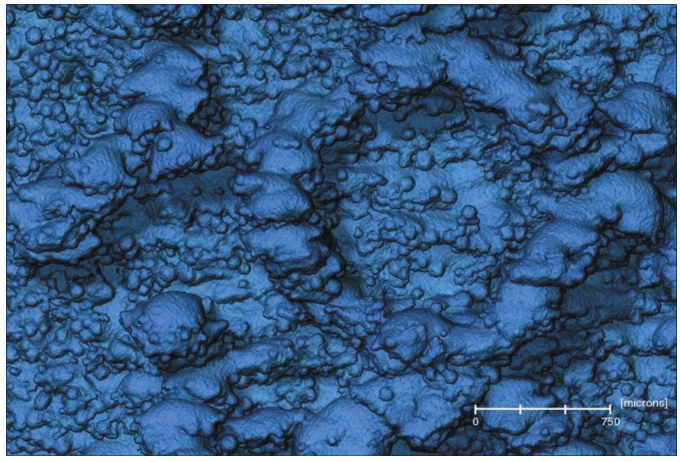

Figure 4
Surface finish variation between the fish tag body and the raised pattern on it.

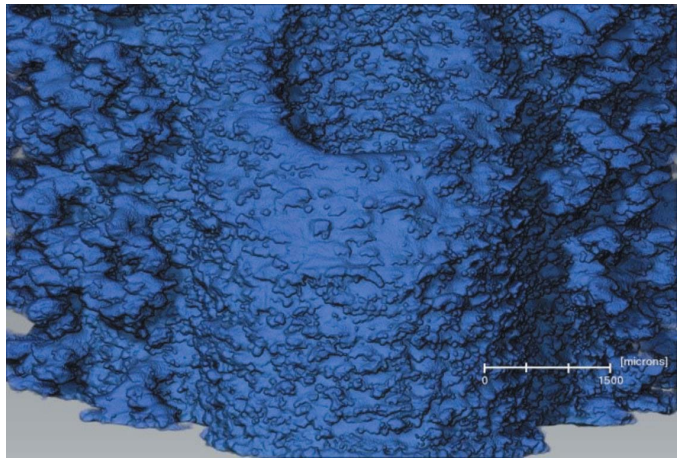

Figure 5
Cylindrical attachment on the side of a shark tag base.

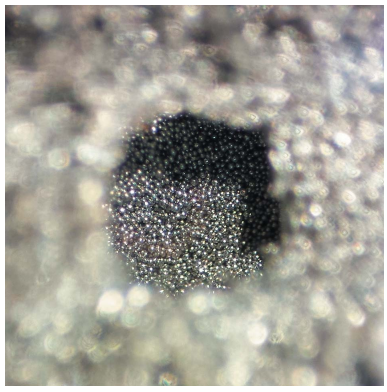

Figure 6
Optical image of the hole in the side of the fish tag showing lightly sintered powder retained following completion of the piece.

upright section to the curved top face as it connects to the main body of the piece. The retained powder morphology is far less apparent as the inward slope moves towards being a final surface. Some of the powder morphology remains at the intersection of overlapping contours as the slope is 'stepped' back towards the main body of the piece.

The fish tag should be hollow inside with a hole through it horizontally. During the build process powder has been trapped within this hollow area (Fig. 6). It is retained in the closed area during the build and has not been removed from the horizontal hole with other loose powder at the finish of the process as it is lightly sintered. Fig. 7 shows a cross section of the piece with the retained powder clearly visible. This retention of powder has also affected the formation of the solid partition across the piece and an example of the ingress can also be seen in the inset in Fig. 7.

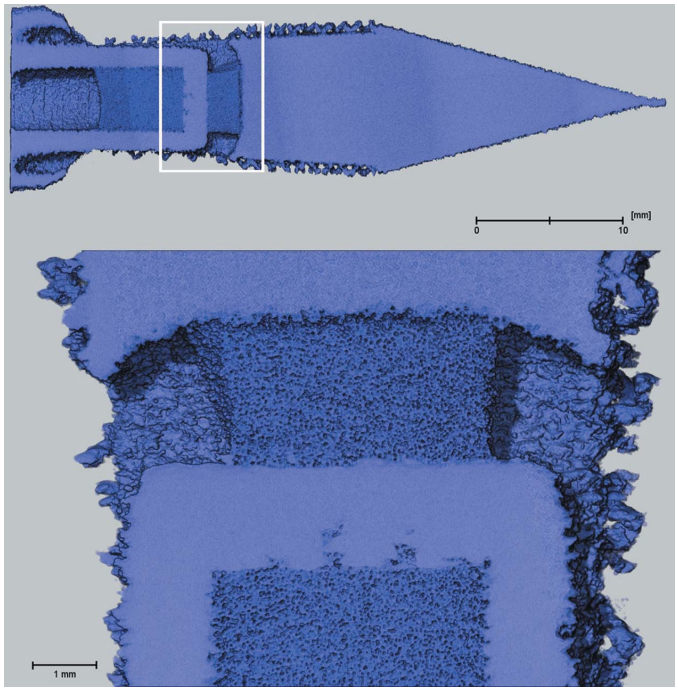

Figure 7
Cross section through the fish tag showing lightly sintered powder permeating the solid partition.

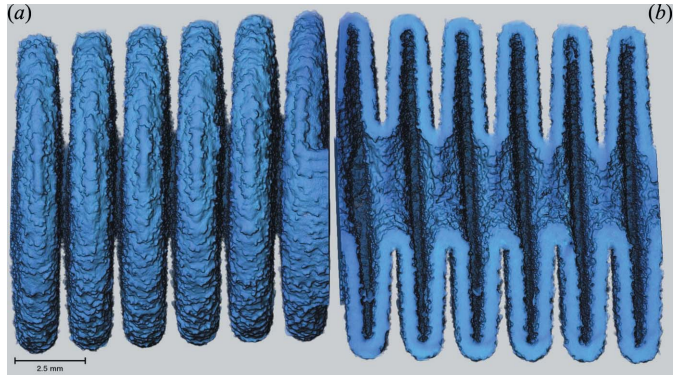

Figure 8
Outer (*a*) and inner (*b*) views of the thick-walled flexible hose section.

3.2. Flexible hose sections

The sections of flexible hosing examined here comprise a series of hollow 'doughnuts' joined through their centres rather than coils of solid wire. Outer and inner views are shown in Fig. 8. The samples vary in the wall thickness of the doughnuts. Neither sample is complete with the build of the thin-walled piece being stopped prematurely and the thick-walled part being sectioned prior to examination.

3.2.1. Thin-walled flexible hose section. Manufacture of the thin-walled flexible hose was stopped part way through the build but approximately half the piece was available for examination. The attempt to produce very thin walls has resulted in large inter- and intra-layer holes (Fig. 9). Positions approximately 90° apart on the outer surface of the hose show smooth features which appear similar to those associated with the upper face of a build; however, it is the other side which

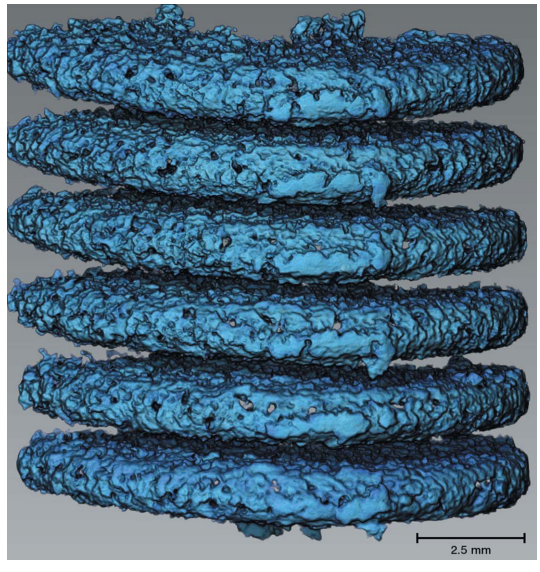

Figure 9
View of the base of the thin-walled hose section showing its smooth morphology and the large inter- and intra-holes throughout the piece.

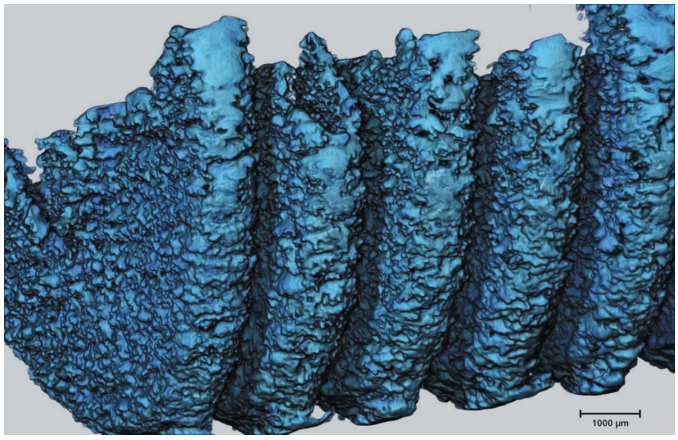

Figure 10
Outer edge of the thin-walled flexible hose approximately 90° from the base showing similar smooth morphology to that seen in Fig. 9.

is actually the top (Fig. 10). This feature of smooth, rounded morphology on the bottom of the piece appears to be a function of designs which do not have sizeable flat areas on the base. The smooth finish on the side is associated with the outer contour moving through its maximum and is produced in a similar fashion to that shown in Fig. 5, *i.e.* a slope moving towards what is effectively a final surface.

There are positions on the planes of the hose's coils where lack of adhesion at one point has prevented adhesion in neighbouring regions. This has led to continuous flaws which extend across several layers (Fig. 11). Features such as these are apparent on the upper and lower planes of each coil.

3.2.2. Thick-walled flexible hose section. The second flexible hose examined here (Fig. 8) was a cut section from a complete sample. The surface morphology has much in common with that of the thin-walled hose, *e.g.* well preserved powder morphology on flat sections and similar smooth features at 90° to the final surface. This latter feature is not as clear as in the thin-walled piece due to the position of the sectioning. Fig. 12 shows an approximation of the layering on the side of one of the coils of such a hose. Note that only the section above the dotted line has been available for examination.

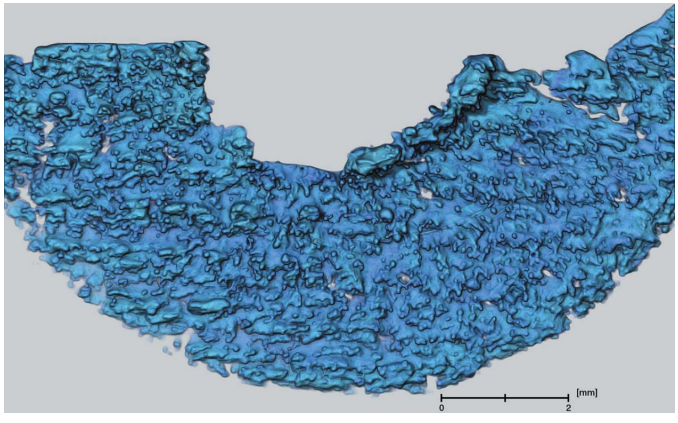

Figure 11
Internal plane of the hose coil showing extended discontinuities in adhesion.

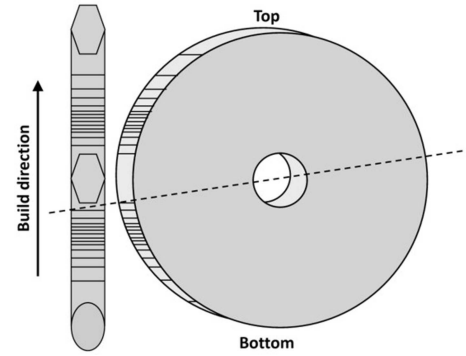

Figure 12
Schematic diagram suggesting the pattern of the layering on the side of the hose coils (not to scale).

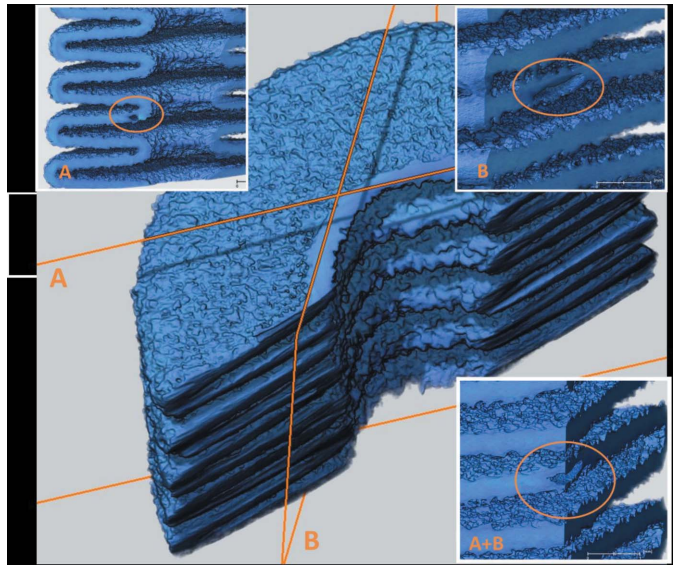

Figure 13
Internal flaw at the intersection of clip planes A and B.

In general, the walls are solid in cross section. However, in some places a lack of adhesion between layers has resulted in an extended flaw which effectively thins the wall. Fig. 13 shows such an internal flaw occurring at the intersection of clipping planes marked A and B in the figure. The inset pictures show the result of clipping each plane singly and also the combined result. Excess material has also been retained within the structure. In this case small sintered pieces of material may be seen both within and between the individual doughnuts (Fig. 14). The pieces of such material observed here have the smooth morphology consistent with a final layer although the build direction is perpendicular to that surface.

3.3. Acetabular cup

An optical image of the complete acetabular cup is shown in Fig. 15. Due to the size of the piece, only a slice through its

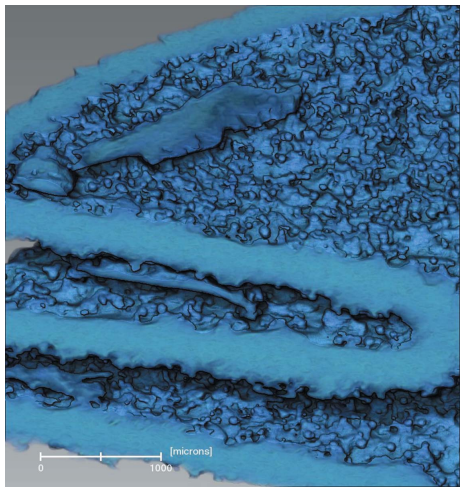

Figure 14
Sintered material caught both between and within the coils of the thick-walled flexible hose.

Figure 15
Optical image of the acetabular cup.

section was imaged. This reduced sampling still resulted in a large, somewhat noisy, dataset. Many of the features apparent here have been previously observed in other samples. The inner and outer surfaces of the upper cylinder (Fig. 16) are similar to that of the conical portion of the fish tag (Fig. 3). The mesh on the outer surface of the acetabular cup (lower left-hand side in Fig. 16) has much the same surface morphology as that of the coarse pattern on the main body of the tag.

Although the bulk of the acetabular cup slice is solid, there are quite large areas (1–2 mm) of interconnected porosity (Fig. 17). These may occur due to lack of fusion both inter- and intra-layer as appears to be the case of the thin-walled flexible hose but the resolution of this experiment is insufficient to determine this. All acetabular cups are put through hot isostatic pressing (HIP) treatments at high temperatures and pressures to seal up such flaws prior to implantation. The beneficial effects of the HIP process on defects and mechanical performance are discussed by Mireles *et al.* (2015) and Svensson & Ackelid (2009), respectively. However, consideration must also be given to the fact that the process coarsens the microstructure and has been seen to reduce yield strength

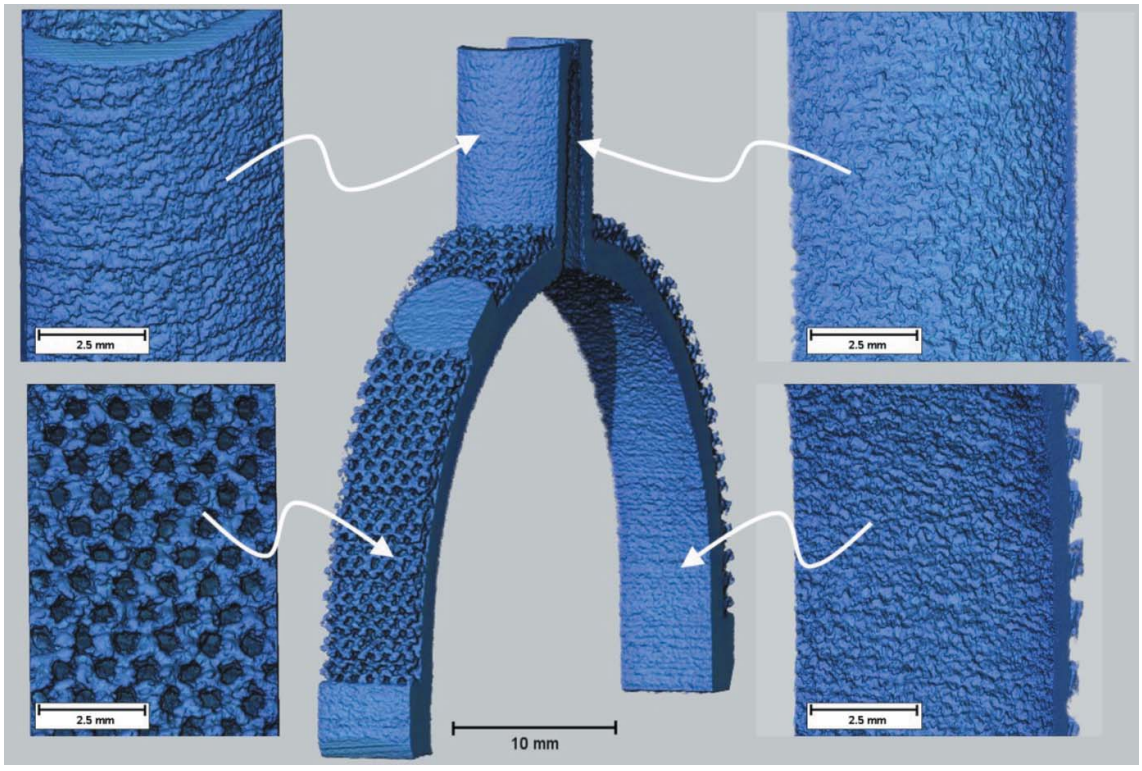

Figure 16
Overview of the surfaces of the acetabular cup slice showing magnified views of outer surfaces on the left-hand side and inner on the right.

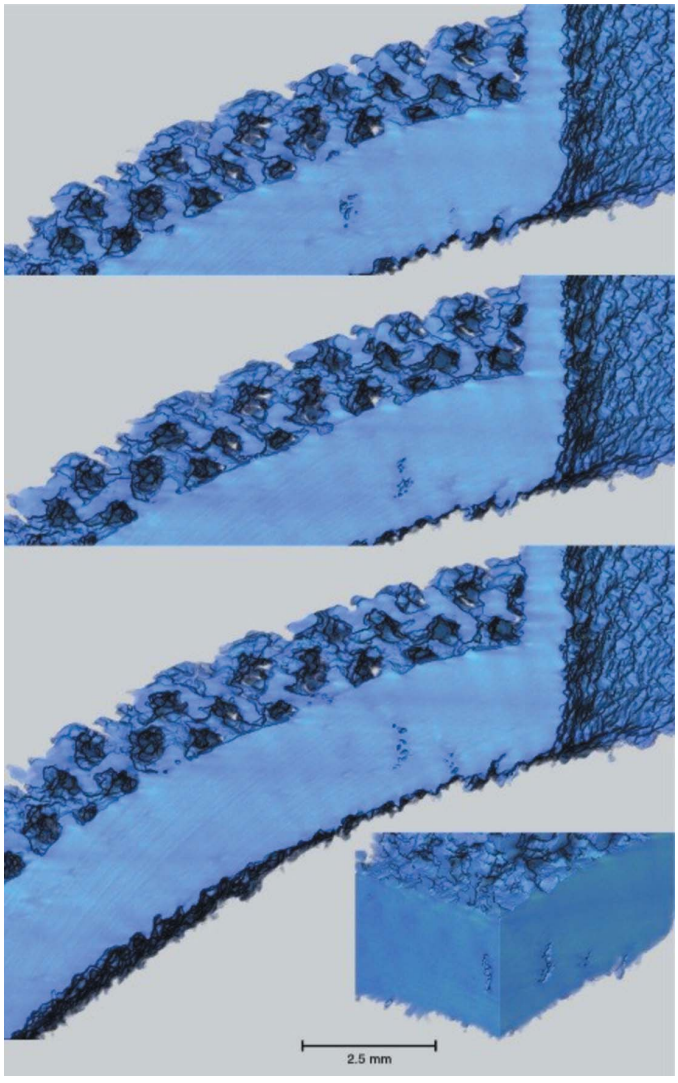

Figure 17
Connected flaws within the acetabular cup. The three upper images show progressive slices through the sample. The image in the lower right-hand corner shows the extent of penetration of the flaws in cross section.

whilst increasing ductility (Mohammadhosseini *et al.*, 2013). It may also slightly increase the roughness of the top surfaces of an EBM part which, as previously described, reduces UTS and yield strength.

3.4. Flat rectangular section

This piece (Fig. 18) was built on supports as an investigation into the conditions needed for the production of large flat areas. Fig. 19 shows the upper surface of the piece and the poor finish that was produced by the long sections of hatching which were oriented diagonally with respect to the supports. The surface is very uneven with many holes/craters in it relating to initial uneven 'bridging' of the hatching across the holes in the support framework. Slicing down through the surface of the rectangle, parallel with the face of the piece, shows a network of connected porosity which does not appear to correlate directly with the pattern of the support (Fig. 20).

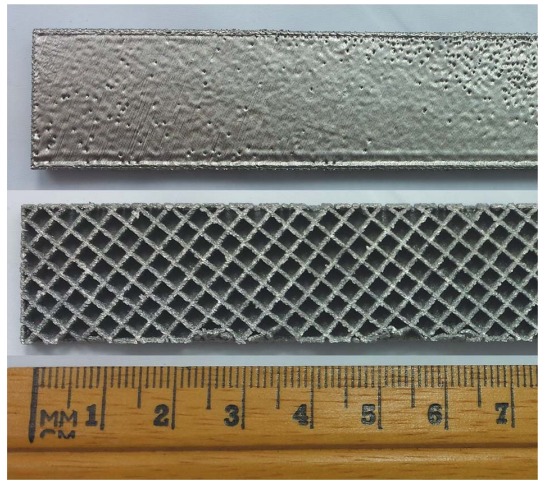

Figure 18
Optical image of long rectangle built on supports (top: final surface; bottom: supports).

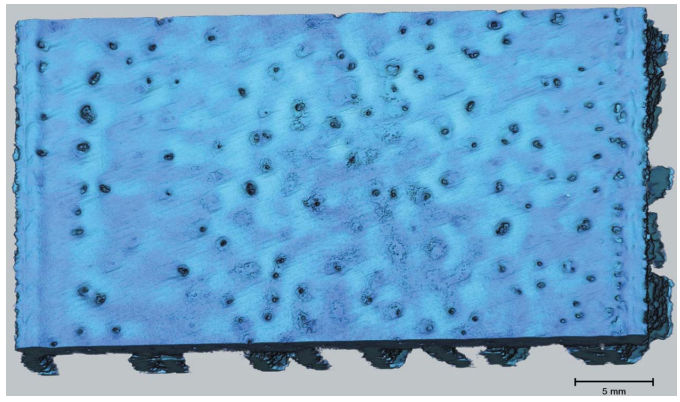

Figure 19
Upper surface of section of long rectangle built on supports.

The opposing edges (left and right sides of Fig. 19) show raised, scalloped edges where the hatching meets the contours. This has been reported previously in Part I (Scarlett *et al.*, 2016), but in this case the diagonally oriented hatching pattern produces a distinct skew on the edges (Fig. 21). There appears to be a slight offset in the hatching with respect to the contour producing a layer which falls slightly short of the contour on one side (Fig. 21*a*) and slightly overhangs the opposing side (Fig. 21*b*). The distortion of the edge is most pronounced on the shortfall side (Fig. 21*a*) but is also apparent on the overhanging side (Fig. 21*b*).

4. Conclusion

The aim of this experiment was to use SXRT to identify and characterize any defects present in a number of titanium parts fabricated by additive manufacturing. In general the densification of these materials appears very high although the spatial resolution of the data was only about 20–30 µm so it is possible that finer porosity may exist (note: finer gas pores of size ∼10 µm have been observed with metallographic tech-

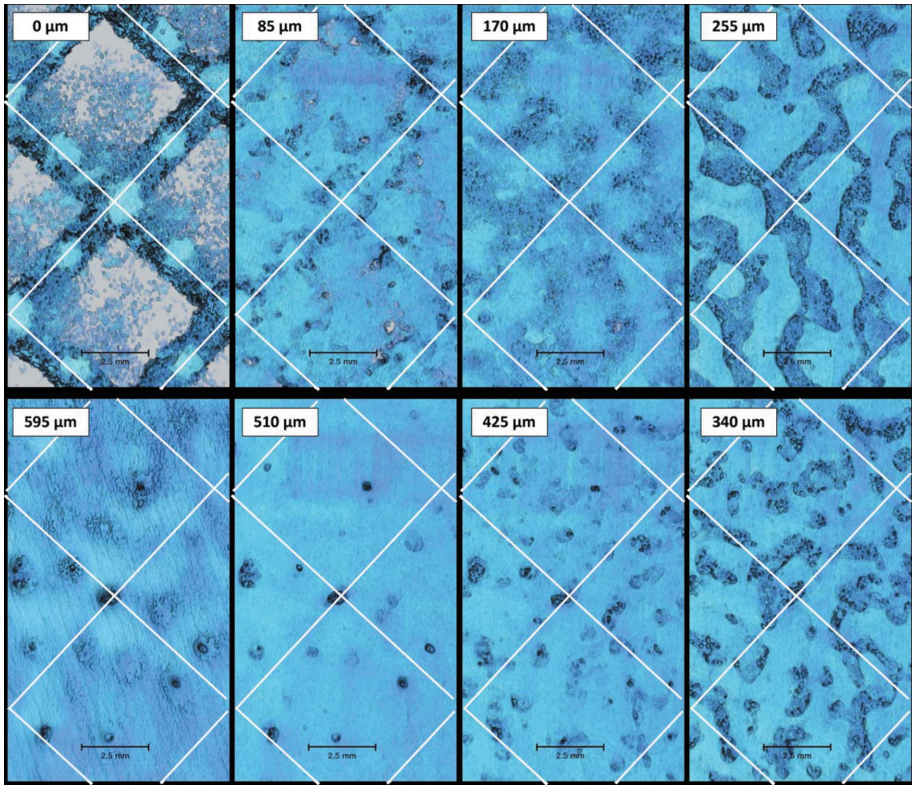

Figure 20
Slices through long rectangle showing the build-up of material on the support (note each is an arbitrary slice and does not represent an integral multiple of material layers as deposited). The view is the same for all the images and the white lines on each denote the location of the supports.

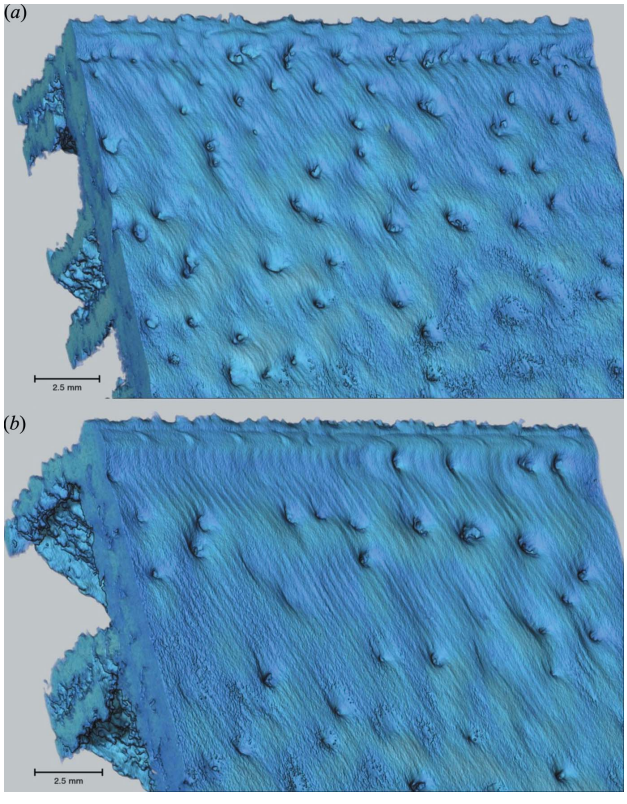

Figure 21
Opposing contours showing raised scalloped edges where the hatching meets the contour.

niques and are a known issue that comes from gas atomization used to make the powder). However, apparently random occurrences of large (∼1–2 mm) holes in some of the pieces was observed. An example of such a case in particular was found in the acetabular cup and appeared to be the agglomeration of a number of smaller holes. This appears to be a lack of fusion linked in a particular area. Avoiding such flaws is obviously desirable although why they occur is unclear.

In the case of the thin-walled flexible hose the thin sheets forming the coils exhibited both inter- and intra-layer lack of adhesion resulting in holes of around 1.5 mm. It appeared that once a flaw had developed in a layer it was generally propagated along that layer or caused a failure of the welding with the subsequent layer. The numerous occurrences of these flaws would seriously affect the resulting strength of the object. Future work would investigate the design thickness needed and/or a modification in parameters for this piece to be built with integrity.

Gas porosity and lack of fusion are a separate issue to that shown in the severely pock-marked surface of the flat rectangular section. This section shows the effect on the final surface of uneven layering which propagates from poor bridging of the supports in the initial layer. This finding has impact on the design of support structures for the building of what are effectively sheet sections.

Complex designs which incorporate cavities and gaps such as the fish tag and the flexible hoses have issues with the retention of lightly sintered powder in holes or the formation and retention of small, generally single layer ‘flakes’ of material between gap surfaces. These may also interfere with the nearby layers as they are deposited. The stability of such weakly adhered material raises questions regarding its potential release in service.

SXRT has revealed a number of defects in the pieces examined here which can be directly related to features in their design. Tomographic examination of complete specimens removes the impact of more traditional inspection *via* sectioning which may miss such features. Knowledge of the existence, prevalence and relative location of such flaws can feed into modified manufacturing protocols to reduce or eliminate their occurrence. This type of information may ultimately be combined with *in situ* monitoring to allow the build protocol to be changed ‘on the fly’ to correct the defect as it occurs (Mireles *et al.*, 2015) or to halt the build if it is irreparable thus saving time and materials and reducing the likelihood of faulty parts entering service.

Acknowledgements

This research was undertaken on the Imaging and Medical Beamline (IMBL) at the Australian Synchrotron, Victoria, Australia. The authors wish to acknowledge the assistance of Dr Andrew Stevenson in preparation for the experiment and Ian Madsen and Helen Brand for their assistance during the experiment.

References

Bourell, D. L., Leu, M. C. & Rosen, D. W. (2009). Editors. *Roadmap for Additive Manufacturing Identifying the Future of Freeform Processing.* The University of Texas at Austin, Texas, USA.

Frazier, W. E. (2014). *J. Materi Eng. Perform.* **23**, 1917–1928.

Gatto, M. & Harris, R. A. (2011). *Rapid Prototyping J.* **17**, 128–137.

Goscinski, W. J., McIntosh, P., Felzmann, U., Maksimenko, A., Hall, C. J., Gureyev, T., Thompson, D., Janke, A., Galloway, G., Killeen, N. E. B., Raniga, P., Kaluza, O., Ng, A., Poudel, G., Barnes, D. G., Nguyen, T., Bonnington, P. & Egan, G. F. (2014). *Front. Neuroinform.* **8**, 30.

Hull, C. W. (1986). *Apparatus for the production of three-dimensional objects by stereolithography*, US Patent US4575330A.

Kodama, H. (1981). *Rev. Sci. Instrum.* **52**, 1770.

Léonard, F., Tammas-Williams, S., Prangnell, P. B., Todd, I. & Withers, P. J. (2012). *Conference on Industrial Computed Tomography (ICT) 2012*, Wels, Austria, pp. 85–93.

Mireles, J., Ridwan, S., Morton, P. A., Hinojos, A. & Wicker, R. B. (2015). *Surface Topogr. Metrol. Properties*, **3**, 189–194.

Mohammadhosseini, A., Fraser, D., Masood, S. H. & Jahedi, M. (2013). *Mater. Res. Innovations*, **17**, S2-106–S2-111.

Scarlett, N. V. Y., Tyson, P., Fraser, D., Mayo, S. C. & Maksimenko, A. (2016). *J. Synchrotron Rad.* **23**, 1006–1014.

Stevenson, A. W., Hall, C. J., Mayo, S. C., Häusermann, D., Maksimenko, A., Gureyev, T. E., Nesterets, Y. I., Wilkins, S. W. & Lewis, R. A. (2012). *J. Synchrotron Rad.* **19**, 728–750.

Sun, Y. Y., Gulizia, S., Oh, C. H., Fraser, D., Leary, M., Yang, Y. F. & Qian, M. (2016). *JOM*, **68**, 791–798.

Svensson, M. & Ackelid, U., (2009) *Medical Device Materials V: Proceedings from the Materials and Processes for Medical Devices Conference 2009*, 10–12 August 2009, Minneapolis, MN, USA, pp. 189–194.

Tammas-Williams, S., Zhao, H., Léonard, F., Derguti, F., Todd, I. & Prangnell, P. B. (2015). *Mater. Charact.* **102**, 47–61.

Thompson, D., Khassapov, A., Nesterets, Y., Gureyev, T. & Taylor, J. (2012). *2012 IEEE 8th International Conference on E-Science (E-Science)*, Chicago, IL, USA.

Van Bael, S., Kerckhofs, G., Moesen, M., Pyka, G., Schrooten, J. & Kruth, J. P. (2011). *Mater. Sci. Eng. A*, **528**, 7423–7431.